Dear Author,

Here are the proofs of your article.

- You can submit your corrections **online**, via **e-mail** or by **fax**.
- For **online** submission please insert your corrections in the online correction form. Always indicate the line number to which the correction refers.
- You can also insert your corrections in the proof PDF and **email** the annotated PDF.
- For fax submission, please ensure that your corrections are clearly legible. Use a fine black pen and write the correction in the margin, not too close to the edge of the page.
- Remember to note the **journal title**, **article number**, and **your name** when sending your response via e-mail or fax.
- **Check** the metadata sheet to make sure that the header information, especially author names and the corresponding affiliations are correctly shown.
- **Check** the questions that may have arisen during copy editing and insert your answers/ corrections.
- **Check** that the text is complete and that all figures, tables and their legends are included. Also check the accuracy of special characters, equations, and electronic supplementary material if applicable. If necessary refer to the *Edited manuscript*.
- The publication of inaccurate data such as dosages and units can have serious consequences. Please take particular care that all such details are correct.
- Please **do not** make changes that involve only matters of style. We have generally introduced forms that follow the journal's style.
  Substantial changes in content, e.g., new results, corrected values, title and authorship are not allowed without the approval of the responsible editor. In such a case, please contact the Editorial Office and return his/her consent together with the proof.
- If we do not receive your corrections **within 48 hours**, we will send you a reminder.
- Your article will be published **Online First** approximately one week after receipt of your corrected proofs. This is the **official first publication** citable with the DOI. **Further changes are, therefore, not possible.**
- The **printed version** will follow in a forthcoming issue.

Please note

After online publication, subscribers (personal/institutional) to this journal will have access to the complete article via the DOI using the URL: http://dx.doi.org/[DOI].
If you would like to know when your article has been published online, take advantage of our free alert service. For registration and further information go to: http://www.link.springer.com.

Due to the electronic nature of the procedure, the manuscript and the original figures will only be returned to you on special request. When you return your corrections, please inform us if you would like to have these documents returned.

Metadata of the article that will be visualized in OnlineFirst

Please note: Images will appear in color online but will be printed in black and white.

ArticleTitle	Identification of two-dimensional pantographic structure via a linear D4 orthotropic second gradient elastic model	
Article Sub-Title		
Article CopyRight	Springer Science+Business Media Dordrecht (This will be the copyright line in the final PDF)	
Journal Name	Journal of Engineering Mathematics	

Corresponding Author	Family Name	**Placidi**
	Particle	
	Given Name	**Luca**
	Suffix	
	Division	
	Organization	Corso Vittorio Emanuele II 39
	Address	00186, Rome, Italy
	Email	luca.placidi@uninettunouniversity.net
	ORCID	http://orcid.org/0000-0002-1461-3997
Author	Family Name	**Andreaus**
	Particle	
	Given Name	**Ugo**
	Suffix	
	Division	
	Organization	Università di Roma La Sapienza
	Address	Rome, Italy
	Email	
	ORCID	
Author	Family Name	**Giorgio**
	Particle	
	Given Name	**Ivan**
	Suffix	
	Division	
	Organization	Università di Roma La Sapienza
	Address	Rome, Italy
	Email	
	ORCID	

	Received	8 July 2015
Schedule	Revised	
	Accepted	6 March 2016

Abstract

A linear elastic second gradient orthotropic two-dimensional solid that is invariant under 90° rotation and for mirror transformation is considered. Such anisotropy is the most general for pantographic structures that are composed of two identical orthogonal families of fibers. It is well known in the literature that the corresponding strain energy depends on nine constitutive parameters: three parameters related to the first gradient part of the strain energy and six parameters related to the second gradient part of the strain energy. In this paper, analytical solutions for simple problems, which are here referred to the heavy sheet, to the nonconventional bending, and to the trapezoidal cases, are developed and presented. On the basis of such analytical solutions, gedanken experiments were developed in such a way that the whole set of the nine constitutive parameters is completely characterized in terms of the materials that the fibers are made of (i.e., of the Young's modulus of the fiber materials), of their cross sections (i.e., of the area and of the moment of inertia of the fiber cross sections), and of the distance between the nearest pivots. On the basis of these considerations, a remarkable form of the strain energy is derived in terms of the displacement fields that closely resembles the strain energy of simple Euler beams. Numerical simulations confirm the validity of the presented results. Classic bone-shaped deformations are derived in standard bias numerical tests and the presence of a floppy mode is also made numerically evident in the present continuum model. Finally, we also show that the largeness of the boundary layer depends on the moment of inertia of the fibers.

Keywords (separated by '-')	Analytical solution - Floppy mode - Identification - Pantographic structures - Second gradient elasticity
Mathematics Subject Classification (separated by '-')	74A30 - 74Q15
Footnote Information	

J Eng Math
DOI 10.1007/s10665-016-9856-8

Identification of two-dimensional pantographic structure via a linear D4 orthotropic second gradient elastic model

Luca Placidi · **Ugo Andreaus** · **Ivan Giorgio**

Received: 8 July 2015 / Accepted: 6 March 2016

Abstract A linear elastic second gradient orthotropic two-dimensional solid that is invariant under 90° rotation and for mirror transformation is considered. Such anisotropy is the most general for pantographic structures that are composed of two identical orthogonal families of fibers. It is well known in the literature that the corresponding strain energy depends on nine constitutive parameters: three parameters related to the first gradient part of the strain energy and six parameters related to the second gradient part of the strain energy. In this paper, analytical solutions for simple problems, which are here referred to the heavy sheet, to the nonconventional bending, and to the trapezoidal cases, are developed and presented. On the basis of such analytical solutions, gedanken experiments were developed in such a way that the whole set of the nine constitutive parameters is completely characterized in terms of the materials that the fibers are made of (i.e., of the Young's modulus of the fiber materials), of their cross sections (i.e., of the area and of the moment of inertia of the fiber cross sections), and of the distance between the nearest pivots. On the basis of these considerations, a remarkable form of the strain energy is derived in terms of the displacement fields that closely resembles the strain energy of simple Euler beams. Numerical simulations confirm the validity of the presented results. Classic bone-shaped deformations are derived in standard bias numerical tests and the presence of a floppy mode is also made numerically evident in the present continuum model. Finally, we also show that the largeness of the boundary layer depends on the moment of inertia of the fibers.

Keywords Analytical solution · Floppy mode · Identification · Pantographic structures · Second gradient elasticity

Mathematics Subject Classification 74A30 · 74Q15

1 Introduction

The aim of this paper is to provide a linear second gradient elastic model for two-dimensional pantographic structures. Pantographic lattices may have an importance in many scientific and applicative sectors, such as in dynamics where the possibility of bandgaps is possible, the biomechanics of fiber reinforcements of growing and reconstructed living

L. Placidi (✉)
Corso Vittorio Emanuele II 39, 00186 Rome, Italy
e-mail: luca.placidi@uninettunouniversity.net

U. Andreaus · I. Giorgio
Università di Roma La Sapienza, Rome, Italy

Journal: 10665-ENGI Article No.: 9856 MS Code: ENGI-D-15-00194.3 TYPESET DISK LE CP Disp.:2016/4/9 Pages: 21 Layout: Medium

tissues, and in piezo- or flexo-electricity. The measurements performed in [1] showed that, starting from the first failure up to the definitive rupture, the energy that is necessary to reach the total rupture is greater than the elastic energy that can be accumulated at maximum. This implies that this microstructure has the ability to generate an extremely tough (meta)material.

At the microlevel, the pantographic structure has a lattice that is composed of two orthogonal families of fibers. The fibers are constituted by cylinders with a given cross-sectional shape. At each intersecting point of the two families, and orthogonal to them, we have a much smaller rod that serves to connect the two families of fibers. At the mesolevel, for each fiber is assumed the validity of the Euler beam model with finite axial resistance, and for each intersecting point of the two families of fibers, it is also assumed that the internal hinge constraint is valid. In this simplified case, the resistance of such internal pivots to the relative rotation among the two families of fibers is assumed to be zero, so that the presence of one floppy mode is considered; see, for example, [2].

At the macrolevel, the continuum model is not isotropic. Pipkin, Steigmann, Eremeyev, and dell'Isola [3–7] have worked on models of this kind. In classic models, if one takes a fiber in a shell (or in a plate) and changes its curvature within the tangent space of the shell (or within the plate), and with reference to the actual configuration, then the elastic energy does not change. This clearly shows the necessity of changing this kind of modeling for pantographic structures because the fibers for sure accumulate strain energy in their bending process. In other words, the so-called geodesic bending should be taken into account [8–10], and we need a model for which it is associated to a change in the elastic energy. Macroscopic models have the advantage of small computational cost. However, microscopic and mesoscopic models can be helpful in the development of a good macroscopic model as well as in the identification of its parameters. In addition, the presence of defects and imperfections at the microscale makes the model at the microlevel very difficult to define. Moreover, because these structures are very thin and light but have a high anisotropic stiffness, buckling and postbuckling phenomena can occur when the structures are subjected to compression or bending deformation. Therefore, for the identification of material parameters, new experiments should be designed very carefully, with an eye toward avoiding critical deformations that could trigger instability (e.g., [11–13]).

Size–scale effects [14–16] cannot be investigated when the mechanics is investigated via a classical approach. In [17] isotropy and microrandomness imply conformal invariance of the curvature. Numerical investigation of pantographic structures requires the development of new techniques [18–26]. In addition, the proper employment of existing methods, for example [27], are used to obtain the dynamics of such a class of microstructured materials.

In the first half of the nineteenth century, Piola [28] already investigated microstructural effects in mechanical systems in his works by means of continuum theories [29–32]. Many strategies can be used with this aim. When strongly localized deformation features are observed [33–39], a suitable theoretical model is given by adding, to the displacement field, additional kinematical descriptors [40–43]. This leads to what is called a micromorphic model [44].

It is also possible to use second- or higher-order gradient theories, where, respectively, the deformation energy is a function of second- or higher-order displacement gradients [45–48]. Such a possibility is accomplished in the literature not only for monophasic [49–54] but also for biphasic (e.g., [55–61]) or granular material [62] systems and in cases of lattice/woven structures [63–65]. An important characteristic of second- and higher-order continua is that, unlike classical Cauchy continua, they can respond to concentrated forces and to other generalized contact actions (e.g., [66]). In addition, new manufacturing procedures, for example 3D printing processes, now allow important applications in terms of a wide class of new materials [67] with a given microstructure (architectured materials). In fact, pantographic structures [68,69] can be 3D printed and experimentally verified. From this point of view, it is observed that the elongation of each fiber can be more than 10 % [70]. This justifies the finite axial resistance at the mesoscale. Moreover, in bias elongation tests, the presence of boundary layers whose lengths are proportional to the moments of inertia of the fibers (see also [71]) and interactions between elongation and bending constitute necessary ingredients of a good model.

In [72], the isotropic strain-gradient model is considered. It appears that, in the linear elasticity case, only four independent moduli appear in the 2D case. This result was confirmed in [73]. In [74], a complete description of the anisotropic (e.g., [75–77]) 2D (see also [78–80]) strain gradient elasticity is given. In this paper we take the

Journal: 10665-ENGI Article No.: 9856 MS Code: ENGI-D-15-00194.3 TYPESET DISK LE CP Disp.:2016/4/9 Pages: 21 Layout: Medium

appropriate kind of orthotropy for linear strain gradient elasticity for pantographic structure. In this context we have three first gradient coefficients and six second gradient coefficients. A complete characterization (or identification [81,82]) of the nine constitutive coefficients for pantographic structures is given. Moreover, the symmetry analysis as performed in [83,84] may be useful for different geometries of fibers, for example for fibers constituting a nonorthogonal lattice.

The method is the same as that used for the isotropic case in [73]. We take a first gradient problem whose solution is known. Then the solution is imposed on the second gradient case and the external actions are explicitly calculated via the boundary conditions. Thus, the set of constitutive parameters is identified via a method that is explained.

2 Formulation of problem

2.1 Definition of deformation energy functional

$\mathcal{B}$ is a 2D body that is considered in the reference configuration, where the X are the coordinates of its points. $U(G, \nabla G)$ is the internal energy density functional that is a function of the deformation matrix $G = \left(F^{\mathrm{T}} F - I\right)/2$ and of its gradient ∇G. Here, $F = \nabla \chi$, where χ is the placement function, F^{T} is the transpose of F, and ∇ is the gradient operator. The energy functional $\mathcal{E}(u(X))$ depends on the displacement $u = \chi - X$ and makes two contributions: the internal and the external energies,

$$\mathcal{E}(u(X)) = \iint_{\mathcal{B}} \left[U(G, \nabla G) - b^{\mathrm{ext}} \cdot u\right] \mathrm{d}A - \int_{\partial\mathcal{B}} \left[t^{\mathrm{ext}} \cdot u + \tau^{\mathrm{ext}} \cdot [(\nabla u) n]\right] \mathrm{d}s - \int_{[\partial\partial\mathcal{B}]} f^{\mathrm{ext}} \cdot u, \tag{1}$$

where n is the unit external normal and the dot $\cdot$ indicates the usual scalar product; b^{ext} is the external body force (per unit area); t^{ext} and τ^{ext} are (per unit length) the external force and double force; and f^{ext} is the external concentrated force, which is applied on the vertices $[\partial\partial\mathcal{B}]$. In other words, the last integral is the sum of the external works made by the concentrated forces applied to the vertices. In addition,

$$\partial\mathcal{B} = \bigcup_{c=1}^{m} \Sigma_c, \quad [\partial\partial\mathcal{B}] = \bigcup_{c=1}^{m} \mathcal{V}_c.$$

Thus, the boundary $\partial\mathcal{B}$ is the union of m regular parts Σ_c (with $c = 1, \ldots, m$), and the so-called boundary of the boundary $[\partial\partial\mathcal{B}]$ is the union of the corresponding m vertex points $\mathcal{V}_c$ (with $c = 1, \ldots, m$) with coordinates X^c. Finally, for the sake of simplicity, we make explicit that the line and vertex integrals of a generic field $g(X)$ are

$$\int_{\partial\mathcal{B}} g(X) \mathrm{d}s = \sum_{c=1}^{m} \int_{\Sigma_c} g(X) \mathrm{d}s, \quad \int_{[\partial\partial\mathcal{B}]} g(X) = \sum_{c=1}^{m} g\left(X^c\right). \tag{2}$$

2.2 Formulation of variational principle

A standard procedure to derive the system of partial differential equations (PDEs) is to assume $\delta\mathcal{E} = 0$ for any kinematically admissible displacement variation δu. Thus, from (1) the procedure to find the minimum of $\mathcal{E}$ is explored, see [85]:

$$\begin{aligned} \delta\mathcal{E} = &- \iint_{\mathcal{B}} \delta u_\alpha \left[\left(F_{\alpha i}\left(S_{ij} - P_{ijh}\right)\right)_{,j} + b_\alpha^{\mathrm{ext}}\right] \mathrm{d}A \\ &+ \int_{\partial\mathcal{B}} \left[\delta u_\alpha \left(t_\alpha - t_\alpha^{\mathrm{ext}}\right) + \delta u_{\alpha,j} n_j \left(\tau_\alpha - \tau_\alpha^{\mathrm{ext}}\right)\right] \mathrm{d}s + \int_{[\partial\partial\mathcal{B}]} \delta u_\alpha \left(f_\alpha - f_\alpha^{\mathrm{ext}}\right). \end{aligned} \tag{3}$$

Journal: 10665-ENGI Article No.: 9856 MS Code: ENGI-D-15-00194.3 TYPESET DISK LE CP Disp.:2016/4/9 Pages: 21 Layout: Medium

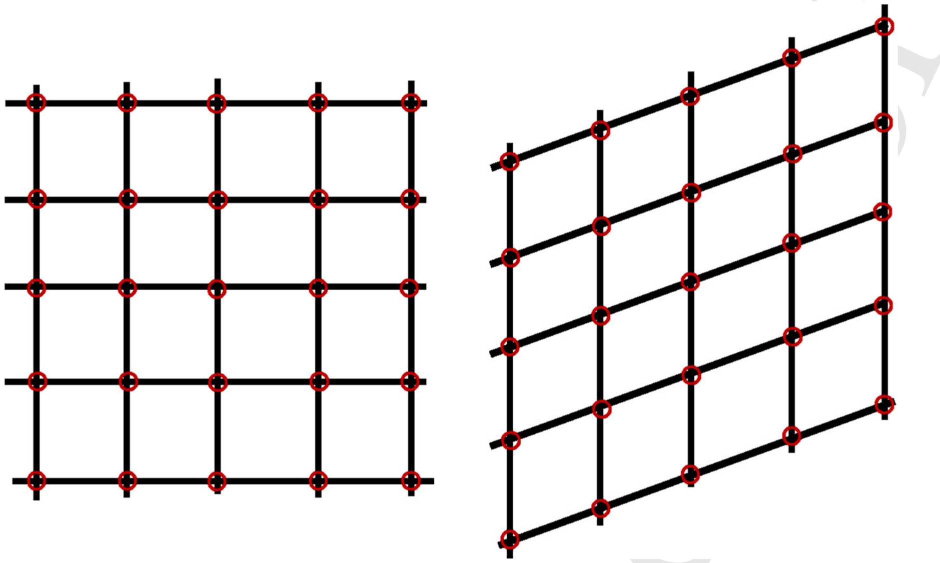

Fig. 1 Discrete pantographic structure. *Left-hand side*: reference configuration; *right-hand side*: deformation in floppy mode condition

For the sake of simplicity, we skip to index notations (the derivative with respect to X_j, which is the jth component of position X, is indicated by the subscript j after a comma; a general rule for index notation: the subscript indices of a symbol denoting a vector or a tensor quantity denote the components of that quantity) and the following positions were used:

$$t_\alpha = F_{\alpha i}\left(S_{ij} - T_{ijh,h}\right)n_j - P_{ka}\left(F_{\alpha i}T_{ihj}P_{ah}n_j\right)_{,k}, \tag{4}$$

$$\tau_\alpha = F_{\alpha i}T_{ijk}n_j n_k, \tag{5}$$

$$f_\alpha = F_{\alpha i}T_{ihj}V_{hj}, \tag{6}$$

where P is the tangential projector operator ($P_{ij} = \delta_{ij} - n_i n_j$), and V is the vertex operator

$$V_{hj} = \nu_h^l n_j^l + \nu_h^r n_j^r,$$

where superscripts l and r refer (roughly speaking, left and right), respectively, to one and the other sides that define a certain vertex point $\mathcal{V}_c$; ν is the external tangent unit vector. The stress and hyperstress tensors are

$$S_{ij} = \frac{\partial U}{\partial G_{ij}}, \quad T_{ijh} = \frac{\partial U}{\partial G_{ij,h}}. \tag{7}$$

2.3 Two-dimensional second gradient orthotropic D_4 linear elasticity

In pantographic structures, the lattice is composed of two orthogonal families of fibers. It is assumed that in the 2D case, for each fiber the Euler beam model with finite axial resistance is valid and for each intersecting point the internal hinge constraint is valid (Fig. 1, left-hand side).

The resistance of such internal pivots to the relative rotation among the two families of fibers is assumed to be zero, so that the presence of one floppy mode is considered (Fig. 1, right-hand side). The equivalent linear elastic continuum model is not isotropic. In the 2D case the collection of symmetry groups is shown in [86]. The equivalent continuum model of a pantographic structure should be invariant for a $\pi/2$ rotation and for a mirror transformation. This symmetry group is denoted by D_4. The internal energy for such a symmetry group is reported in Appendices A and B of [74]. The derivation of these equations is not straightforward; it is done explicitly in [87]; see also the

Journal: 10665-ENGI Article No.: 9856 MS Code: ENGI-D-15-00194.3 TYPESET DISK LE CP Disp.:2016/4/9 Pages: 21 Layout: Medium

related works [88,89]. In particular, the reader is encouraged to refer to Eq. (50) of Ref. [87] and the internal energy density functional $U(G, \nabla G)$ is as follows:

$$U(G, \nabla G) = \hat{U}(\epsilon, \eta) = \frac{1}{2} C_{IJ} \epsilon_I \epsilon_J + \frac{1}{2} A_{\alpha\beta} \eta_\alpha \eta_\beta, \tag{8}$$

where the indices I and J vary from 1 to 3, the indices α and β vary from 1 to 6, ϵ_I is the Ith component of the column vector ϵ

$$\epsilon = \begin{pmatrix} G_{11} \\ G_{22} \\ \sqrt{2} G_{12} \end{pmatrix}, \tag{9}$$

η_α is the αth component of the column vector η

$$\eta = \begin{pmatrix} G_{11,1} \\ G_{22,1} \\ \sqrt{2} G_{12,2} \\ G_{22,2} \\ G_{11,2} \\ \sqrt{2} G_{12,1} \end{pmatrix}, \tag{10}$$

C_{IJ} is the IJth component of the 3×3 matrix C,

$$C = \begin{pmatrix} c_{11} & c_{12} & 0 \\ c_{12} & c_{11} & 0 \\ 0 & 0 & c_{33} \end{pmatrix}, \tag{11}$$

and $A_{\alpha\beta}$ is the $\alpha\beta$th component of the matrix A,

$$A = \begin{pmatrix} a_{11} & a_{12} & a_{13} & 0 & 0 & 0 \\ a_{12} & a_{22} & a_{23} & 0 & 0 & 0 \\ a_{13} & a_{23} & a_{33} & 0 & 0 & 0 \\ 0 & 0 & 0 & a_{11} & a_{12} & a_{13} \\ 0 & 0 & 0 & a_{12} & a_{22} & a_{23} \\ 0 & 0 & 0 & a_{13} & a_{23} & a_{33} \end{pmatrix}. \tag{12}$$

In this class of orthotropic materials, the isotropic classic two Lamè coefficients λ and μ are replaced by the three coefficients c_{11}, c_{12}, and c_{33}. In addition, the four isotropic coefficients are replaced by the six coefficients a_{11}, a_{12}, a_{13}, a_{22}, a_{23}, and a_{33}. The bulk modulus κ and the shear modulus μ are the most convenient pair of elastic constants for an isotropic material [90–98]. Nevertheless, we prefer to write the density of the deformation energy in (8) in terms of the Lamè coefficients λ and μ.

The positive definiteness of matrices C and A assures the positive definiteness of U. To do this, it is sufficient to calculate the eigenvalues of both matrices and impose a restriction on their positivity. The eigenvalues λ_1^C, λ_2^C, and λ_3^C of matrix C are easy to calculate,

$$\lambda_1^C = c_{33}, \quad \lambda_2^C = c_{11} - c_{12}, \quad \lambda_3^C = c_{11} + c_{12},$$

and a restriction on their positivity means

$$c_{33} > 0, \quad c_{11} > c_{12}, \quad c_{11} > -c_{12}. \tag{13}$$

Journal: 10665-ENGI Article No.: 9856 MS Code: ENGI-D-15-00194.3 TYPESET DISK LE CP Disp.:2016/4/9 Pages: 21 Layout: Medium

The eigenvalues λ_1^A, λ_2^A, and λ_3^A of matrix A in (12) are the same as that of its submatrix A_1:

$$A_1 = \begin{pmatrix} a_{11} & a_{12} & a_{13} \\ a_{12} & a_{22} & a_{23} \\ a_{13} & a_{23} & a_{33} \end{pmatrix}.$$

Their analytical derivation is not straightforward because it requires an analytical solution of a third-order polynomial equation. Such a derivation is certainly possible, but the results would occupy too much space. Thus, we can formally write a condition for positive definiteness as follows:

$$\lambda_1^A > 0, \quad \lambda_2^A > 0, \quad \lambda_3^A > 0. \tag{14}$$

The presence of a floppy mode has the consequence of relaxing these conditions in such a way that semipositive definiteness is accepted. In other words, the equal sign is accepted in restrictions (13) and (14). In particular, we will show in (62), and therefore in the representation (65), that the identification of a pantographic structure implies $c_{33} = 0$, so that the first inequality of (13) is in fact relaxed to become $c_{33} \geq 0$. Moreover, an explicit representation of the eigenvalues λ_1^A, λ_2^A, and λ_3^A with the identification of the pantographic structure can easily be evaluated from (65):

$$\lambda_1^A = 0, \quad \lambda_2^A = 0, \quad \lambda_3^A = 3\frac{E_m I_m}{d_m} > 0.$$

Even in this case, the need to relax the conditions $(14)_1$ and $(14)_2$, so that the equal sign is accepted for pantographic structures, becomes evident.

The system of PDEs can be deduced by the first line of (3). Here, it is made explicit:

$$\begin{aligned} c_{11}u_{1,11} + \frac{1}{2}c_{33}\left(u_{1,22} + u_{2,12}\right) + c_{12}u_{2,12} = {} & a_{11}u_{1,1111} + \frac{1}{\sqrt{2}}(a_{13} + a_{23})\left(u_{2,1222} + u_{2,1112} + 2u_{1,1122}\right) \\ & + a_{22}u_{1,1122} + a_{12}\left(u_{2,1222} + u_{2,1112}\right) \\ & + \frac{1}{2}a_{33}\left(u_{1,2222} + u_{1,1122} + u_{2,1222} + u_{2,1112}\right) - b_1^{\text{ext}} \end{aligned} \tag{15}$$

$$\begin{aligned} c_{11}u_{2,22} + \frac{1}{2}c_{33}\left(u_{2,11} + u_{1,12}\right) + c_{12}u_{1,12} = {} & a_{11}u_{2,2222} + \frac{1}{\sqrt{2}}(a_{13} + a_{23})\left(u_{1,1222} + u_{1,1112} + 2u_{2,1122}\right) \\ & + a_{22}u_{2,1122} + a_{12}\left(u_{1,1222} + u_{1,1112}\right) \\ & + \frac{1}{2}a_{33}\left(u_{2,1111} + u_{2,1122} + u_{1,1112} + u_{1,1222}\right) - b_2^{\text{ext}}. \end{aligned} \tag{16}$$

An interchange of indices 1 and 2 in the displacement field u_i and in the external force per unit area b_i^{ext} in (15), because of the symmetry D_4 , gives Eq. (16), and vice versa.

3 The case of a rectangle

In this section we define the case of a rectangular body. The reason for this choice is twofold. First, all boundaries are straight. This means that the external normals do not depend on the space coordinate X, and therefore – see, for example, Eq. (4) – the boundary conditions are simplified. Second, the presence of vertices implies an increasing number of possible coefficient identifications. The reason is that vertex-boundary conditions, as we will see, must be considered.

3.1 General framework of straight lines

In Fig. 2 the scheme of a rectangle is represented. Side names are A, B, C, and D and vertex names $\mathcal{V}_1$, $\mathcal{V}_2$, $\mathcal{V}_3$, and $\mathcal{V}_4$. In these hypotheses, (4), (5), and (6) are simplified,

$$t_\alpha = S_{\alpha j}n_j - \left(T_{\alpha jh,h} + T_{\alpha hj,h}\right)n_j + T_{\alpha hj,k}n_h n_k n_j, \quad \tau_\alpha = T_{\alpha jk}n_j n_k, \quad f_\alpha = T_{\alpha ij}V_{ij}, \tag{17}$$

Journal: 10665-ENGI Article No.: 9856 MS Code: ENGI-D-15-00194.3 TYPESET DISK LE CP Disp.:2016/4/9 Pages: 21 Layout: Medium

and we have

$$
\begin{aligned}
t_1 = {} & c_{11}u_{1,1}n_1 + c_{12}u_{2,2}n_1 + \frac{c_{33}}{2}\big(u_{1,2}+u_{2,1}\big)n_2 - a_{11}n_1\big(u_{1,112}n_2 + u_{1,111}(2+n_1n_1)\big)\\
& - a_{12}\big(u_{2,222}n_1(1+n_2n_2) + u_{2,122}n_2(1+2n_1n_1) + u_{2,112}n_1(2+n_1n_1)\big)\\
& - \frac{a_{13}}{\sqrt{2}}n_1\big(u_{1,222}n_1n_2 + u_{2,222}(1+n_2n_2) + u_{1,122}(2+n_1n_1) + u_{2,112}(2+n_1n_1) + u_{1,111}n_2n_2\big)\\
& - \frac{a_{13}}{\sqrt{2}}u_{1,112}n_2(2+n_2n_2) - \frac{a_{23}}{\sqrt{2}}n_1\big(u_{1,122}2(1+n_2n_2) + u_{2,112}(1+2n_2n_2)\big)\\
& - \frac{a_{23}}{\sqrt{2}}n_2\big(u_{2,122}(2+n_2n_2) + u_{1,112}2(1+n_1n_1) + u_{2,111}(1+n_1n_1)\big)\\
& - \frac{a_{33}}{2}n_1\big(u_{1,122}(1+2n_2n_2) + u_{2,112}(1+2n_2n_2)\big)\\
& - \frac{a_{33}}{2}n_2\big(u_{1,222}(2+n_2n_2) + u_{2,122}(2+n_2n_2) + u_{1,112}(1+n_1n_1) + u_{2,111}(1+n_1n_1)\big)
\end{aligned} \tag{18}
$$

$$
\begin{aligned}
\tau_1 = {} & a_{11}u_{1,11}n_1n_1 + a_{12}n_1\big(u_{2,22}n_2 + u_{2,12}n_1\big)\\
& + \frac{a_{13}}{\sqrt{2}}\big(u_{1,22}n_1n_1 + u_{2,22}n_1n_2 + u_{2,12}n_1n_1 + u_{1,11}n_2n_2\big) + a_{22}u_{1,12}n_1n_2\\
& + \frac{a_{23}}{\sqrt{2}}n_2\big(2u_{1,12}n_1 + u_{2,12}n_2 + u_{2,11}n_1\big) + \frac{a_{33}}{2}n_2\big(u_{1,22}n_2 + u_{1,12}n_1 + u_{2,12}n_2 + u_{2,11}n_1\big)
\end{aligned} \tag{19}
$$

in terms of the displacement fields. Because of the symmetry D_4, an interchange of indices 1 and 2 in the displacement field u_i and in the external unit normal n_i in (18) and in (19) gives, respectively, the force t_2 per unit length and the double force τ_2 per unit length in the other direction in the same way (15) gives Eq. (16) and vice versa. This is why we do not explicitly write out the expressions of the force t_2 per unit length and of the double force τ_2 per unit length.

3.2 Sides and vertices

The characterizations of sides A, B, C, and D is done by inserting into (18) and (19) the unit norms $n_i = -\delta_{i1}$, $n_i = \delta_{i2}$, $n_i = \delta_{i1}$, and $n_i = -\delta_{i2}$, respectively.

The last term of (3) is reduced, because of $(2)_2$, to

$$
\begin{aligned}
\int_{[\partial\partial\mathcal{B}]} \delta u_\alpha\big(f_\alpha - f_\alpha^{\text{ext}}\big) = {} & \big[\delta u_\alpha\big(T_{\alpha ij}V_{ij} - f_\alpha^{\text{ext}}\big)\big]_{\mathcal{V}_1} + \big[\delta u_\alpha\big(T_{\alpha ij}V_{ij} - f_\alpha^{\text{ext}}\big)\big]_{\mathcal{V}_2}\\
& + \big[\delta u_\alpha\big(T_{\alpha ij}V_{ij} - f_\alpha^{\text{ext}}\big)\big]_{\mathcal{V}_3} + \big[\delta u_\alpha\big(T_{\alpha ij}V_{ij} - f_\alpha^{\text{ext}}\big)\big]_{\mathcal{V}_4}.
\end{aligned} \tag{20}
$$

For vertex $\mathcal{V}_1$ side A has $n_j = -\delta_{1j}$ and $\nu_i = \delta_{i2}$ and side B has $n_j = \delta_{2j}$ and $\nu_i = -\delta_{i1}$, so that

$$
\big[V_{ij}\big]_{\mathcal{V}_1} = \Big[\nu_i^l n_j^l + \nu_i^r n_j^r\Big]_{\mathcal{V}_1} = -\delta_{i2}\delta_{1j} - \delta_{i1}\delta_{2j}.
$$

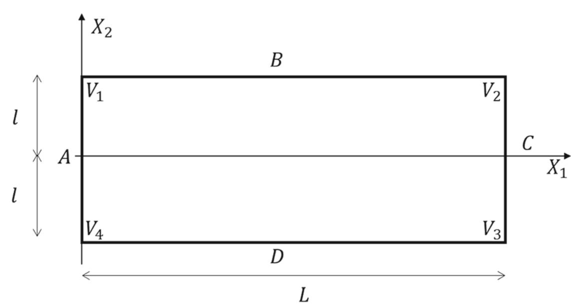

Fig. 2 Nomenclature of 2D body $\mathcal{B}$

Journal: 10665-ENGI Article No.: 9856 MS Code: ENGI-D-15-00194.3 ☐ TYPESET ☐ DISK ☐ LE ☐ CP Disp.:2016/4/9 Pages: 21 Layout: Medium

For vertex $\mathcal{V}_2$ side B has $n_j = \delta_{2j}$ and $\nu_i = \delta_{i1}$ and side C has $n_j = \delta_{1j}$ and $\nu_i = \delta_{i2}$, so that

$$\left[V_{ij}\right]_{\mathcal{V}_2} = \left[\nu_i^l n_j^l + \nu_i^r n_j^r\right]_{\mathcal{V}_2} = \delta_{i1}\delta_{2j} + \delta_{i2}\delta_{1j}.$$

For vertex $\mathcal{V}_3$ side C has $n_j = \delta_{1j}$ and $\nu_i = -\delta_{i2}$ and side D has $n_j = -\delta_{2j}$ and $\nu_i = \delta_{i1}$, so that

$$\left[V_{ij}\right]_{\mathcal{V}_3} = \left[\nu_i^l n_j^l + \nu_i^r n_j^r\right]_{\mathcal{V}_3} = -\delta_{i2}\delta_{1j} - \delta_{i1}\delta_{2j}.$$

For vertex $\mathcal{V}_4$ side D has $n_j = -\delta_{2j}$ and $\nu_i = -\delta_{i1}$ and side A has $n_j = -\delta_{1j}$ and $\nu_i = -\delta_{i2}$, so that

$$\left[V_{ij}\right]_{\mathcal{V}_4} = \left[\nu_i^l n_j^l + \nu_i^r n_j^r\right]_{\mathcal{V}_4} = \delta_{i1}\delta_{2j} + \delta_{i2}\delta_{1j}.$$

Thus, finally, (20) yields

$$\begin{aligned}\int_{[\partial\partial\mathcal{B}]} \delta u_\alpha \left(f_\alpha - f_\alpha^{\text{ext}}\right) &= \left[\delta u_\alpha \left(-T_{\alpha 21} - T_{\alpha 12} - f_\alpha^{\text{ext}}\right)\right]_{\mathcal{V}_1} + \left[\delta u_\alpha \left(T_{\alpha 12} + T_{\alpha 21} - f_\alpha^{\text{ext}}\right)\right]_{\mathcal{V}_2} \\ &\quad + \left[\delta u_\alpha \left(-T_{\alpha 21} - T_{\alpha 12} - f_\alpha^{\text{ext}}\right)\right]_{\mathcal{V}_3} + \left[\delta u_\alpha \left(T_{\alpha 12} + T_{\alpha 21} - f_\alpha^{\text{ext}}\right)\right]_{\mathcal{V}_4},\end{aligned} \tag{21}$$

where $T_{\alpha 12} + T_{\alpha 21}$, in terms of the displacement field, is, for $\alpha = 1$,

$$T_{112} + T_{121} = \left(a_{22} + \sqrt{2}a_{23} + \frac{a_{33}}{2}\right)u_{1,12} + \left(\sqrt{2}a_{23} + \frac{a_{33}}{2}\right)u_{2,11} + \left(a_{12} + \frac{\sqrt{2}}{2}a_{13}\right)u_{2,22}, \tag{22}$$

and, for $\alpha = 2$,

$$T_{212} + T_{221} = \left(a_{22} + \sqrt{2}a_{23} + \frac{a_{33}}{2}\right)u_{2,12} + \left(\sqrt{2}a_{23} + \frac{a_{33}}{2}\right)u_{1,22} + \left(a_{12} + \frac{\sqrt{2}}{2}a_{13}\right)u_{1,11}, \tag{23}$$

where we again note, because of the symmetry D_4, the same characteristics for the interchange of the indices of the displacement field u_i. In other words, we remark again that Eq. (23) is derived from (22) by interchanging the indices of the displacement field u_i and of its derivatives.

3

3.3 Heavy sheet: an analytical solution

The rectangle in Fig. 2 is now considered heavy (a heavy sheet) and hanged by the top side B. The word *heavy* corresponds to a weight loading, i.e., a constant distributed force in the vertical direction and directed downward. The kinematic constraints on the displacement field exclude the kinematic effects of the Poisson effect, in the sense that no lateral displacement is admissible at either vertical side, where horizontal forces must be prescribed. In the next section, we will use the fact that in pantographic strictures (see also the right-hand side of Fig. 3), such a horizontal force is apparently zero.

Thus, the needed kinematic constraints on the horizontal side B and on the two vertical sides A and C are

$$(\delta u_2)_B = 0, \quad (\delta u_1)_A = 0, \quad (\delta u_1)_C = 0. \tag{24}$$

As a result, the top side of the rectangle cannot displace vertically and neither the vertical left- nor right-hand side can displace horizontally; see also Fig. 3. In what follows we proceed as in [73]. Thus, we consider the general solution of the anisotropic first gradient case and we calculate the set of boundary conditions we need, in the second gradient case, to obtain the same solution.

Accordingly, the following displacement field is considered:

$$u_1 = 0, \quad u_2 = \frac{\rho g (X_2 - l)(3l + X_2)}{2c_{11}}. \tag{25}$$

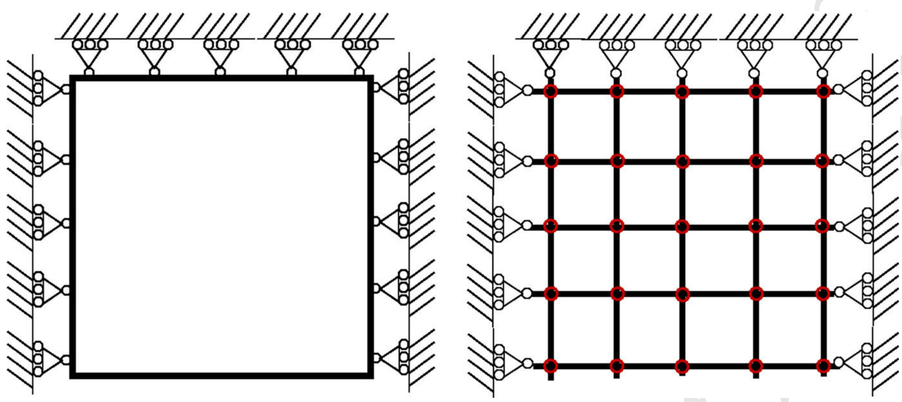

Fig. 3 Heavy sheet gedanken experiment. Continuum *left-hand side* and discrete *right-hand side* points of view

The two PDEs (15) and (16) are satisfied by an external force per unit area,

$$b_1^{\text{ext}} = 0, \quad b_2^{\text{ext}} = -\rho g, \tag{26}$$

that is due to the weight. We have used the following intermediate results:

$$u_{2,2} = \frac{\rho g (l + X_2)}{c_{11}}, \quad u_{2,22} = \frac{\rho g}{c_{11}}. \tag{27}$$

We now calculate the edge forces that are necessary to have the displacement field (25). The apex with letter A, B, C, or D refers to the name of the edge according to the nomenclature in Fig. 2.

From (18) and (25) we have

$$t_1 = t_1^{\text{ext},A} = -\frac{\rho g (l + X_2)}{c_{11}} c_{12}, \quad t_1 = t_1^{\text{ext},C} = \frac{\rho g (l + X_2)}{c_{11}} c_{12}. \tag{28}$$

This horizontal force is a static consequence of the Poisson effect and is associated to the kinematic constraint $(24)_3$. From (18) we have simply

$$t_2 = t_2^{\text{ext},A} = 0, \quad t_2 = t_2^{\text{ext},C} = 0.$$

From (18) and (25) we have

$$t_1 = t_1^B = 0, \quad t_1 = t_1^D = 0,$$

i.e., no shear condition in the horizontal sides, and

$$t_2 = t_2^B = \rho g (l + X_2)_{x_2 = l} = 2\rho g l, \quad t_2 = t_2^D = -\rho g (l + X_2)_{X_2 = -l} = 0. \tag{29}$$

The $(29)_1$ is the expected reaction at the upper boundary. The $(29)_2$ means that there is no reaction at the bottom of the body.

Following the evaluation of the forces per unit length, we now calculate the analogous double force per unit length. In this case as well, an apex with letter A, B, C, or D refers to the name of the edge according to the nomenclature in Fig. 2.

From (19) and (25) we simply have

$$\tau_1 = \tau_1^{\text{ext},A} = 0, \quad \tau_1 = \tau_1^{\text{ext},C} = 0,$$

Journal: **10665-ENGI** Article No.: **9856** MS Code: **ENGI-D-15-00194.3** ☐ TYPESET ☐ DISK ☐ LE ☐ CP Disp.:**2016/4/9** Pages: **21** Layout: **Medium**

i.e., no double force condition in the horizontal direction for the vertical sides. On the other hand, in the vertical direction we have

$$\tau_2 = \tau_2^{\text{ext},A} = \frac{a_{13}\rho g}{\sqrt{2}c_{11}}, \quad \tau_2 = \tau_2^{\text{ext},C} = \frac{a_{13}\rho g}{\sqrt{2}c_{11}}. \tag{30}$$

From (19) and (25) we have

$$\tau_1 = \tau_1^{\text{ext},B} = 0, \quad \tau_1 = \tau_1^{\text{ext},D} = 0,$$

i.e., no double force condition in the horizontal direction for the horizontal sides, and we also have

$$\tau_2 = \tau_2^{D,\text{ext}} = \frac{\rho g a_{11}}{c_{11}}, \quad \tau_2 = \tau_2^{B,\text{ext}} = \frac{\rho g a_{11}}{c_{11}}. \tag{31}$$

To keep the displacement field in (25), the wedge force is, from (21), (22), and (23),

$$f_\alpha^{\text{ext}} = -T_{\alpha 12} - T_{\alpha 21}$$

for wedges $\mathcal{V}_1$ and $\mathcal{V}_3$, and the converse

$$f_\alpha^{\text{ext}} = T_{\alpha 12} + T_{\alpha 21}$$

for wedges $\mathcal{V}_2$ and $\mathcal{V}_4$. We have from (22), (25), and (27)

$$T_{112} + T_{121} = \frac{\left(2a_{12} + \sqrt{2}a_{13}\right)\rho g}{2c_{11}}, \tag{32}$$

and from (23) and (25) and (27)

$$T_{212} + T_{221} = 0.$$

3.4 An analytical solution for nonconventional bending

Let us take into account the displacement field

$$u_1 = 0, \quad u_2 = -\frac{aX_1^2}{2}, \tag{33}$$

which represents a nonconventional bending field (see also Fig. 4). The two PDEs (15) and (16) are satisfied by the following external force per unit area:

$$b_1^{\text{ext}} = 0, \quad b_2^{\text{ext}} = -\frac{a}{2}c_{33}. \tag{34}$$

Let us now explain why we call this kind of deformation a *nonconventional bending*. It is true, in fact, that, for each horizontal microbeam, the bending condition that is achieved is conventional. However, at the macroscale the pantographic sheet deformation is completely different. For example, the direction of each vertical fiber remains invariant, i.e., the vertical fibers do not rotate at all, and does not follow the direction of the horizontal fibers as in the classical conventional bending case, where both horizontal and vertical fibers remain orthogonal to each other.

Journal: 10665-ENGI Article No.: 9856 MS Code: ENGI-D-15-00194.3 TYPESET DISK LE CP Disp.:2016/4/9 Pages: 21 Layout: Medium

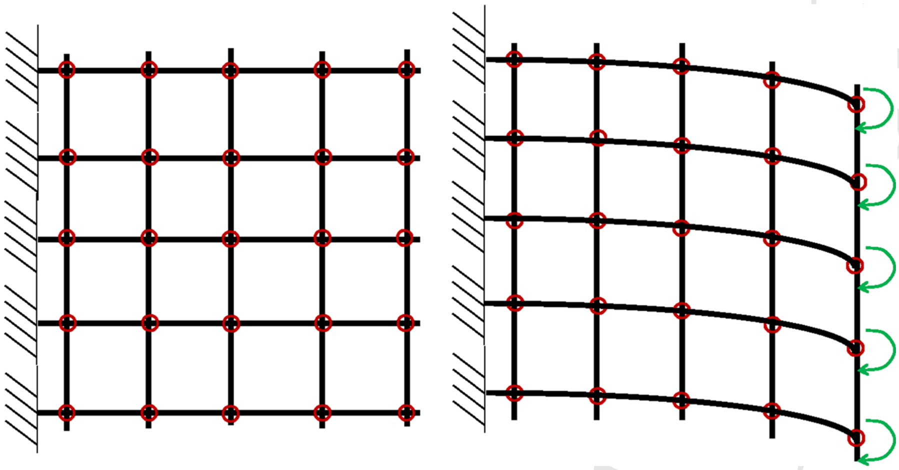

Fig. 4 Discrete pantographic structure in nonconventional bending case. *Left-hand side*: reference configuration; *right-hand side*: deformation in nonconventional bending condition

In what follows we calculate the edge forces that are necessary to have the displacement field (33). Even in this case the apex with letter A, B, C, or D refers to the name of the edge according to the nomenclature in Fig. 2.

From (18) and (33) we have

$$t_1 = t_1^{\text{ext},A} = \frac{aL}{2}c_{33}, \quad t_2 = t_2^{\text{ext},A} = 0, \tag{35}$$

and

$$t_1 = t_1^{\text{ext},C} = -\frac{aL}{2}c_{33}, \quad t_2 = t_2^{\text{ext},C} = 0. \tag{36}$$

For reasons of symmetry, the force on side A is the opposite of that on side C.

From (18) we have no traction conditions in the vertical direction,

$$t_2^{\text{ext},B} = t_2^{\text{ext},D} = 0,$$

for horizontal sides and a nonnull shear condition,

$$t_1^{\text{ext},B} = -t_1^{\text{ext},D} = -\frac{aX_1}{2}c_{33}, \tag{37}$$

in the horizontal direction for the horizontal sides. Again we remark that, for reasons of symmetry, the force on side B is the opposite of that on side D. Now we calculate the double force per unit length and use the same convention to characterize each edge.

From (19) and (33) we simply have

$$\tau_1 = \tau_1^{\text{ext},C} = 0,$$

and we also have

$$\tau_2 = \tau_2^{\text{ext},C} = -\frac{a_{33}}{2}a. \tag{38}$$

Journal: 10665-ENGI Article No.: 9856 MS Code: ENGI-D-15-00194.3 TYPESET DISK LE CP Disp.:2016/4/9 Pages: 21 Layout: Medium

We remark that the force per unit length on this side is zero. Thus the total external moment M_C^{ext} on side C is only due to the double force $\tau_2^{\text{ext},C}$ of (38),

$$M_C^{\text{ext}} = \int_{-l}^{l} \tau_2^{\text{ext},C} \mathrm{d}s = -\frac{a_{33}}{2} a \int_{-l}^{l} \mathrm{d}s = -a_{33} a l, \tag{39}$$

which gives an interpretation of the parameter a introduced in (33), i.e.,

$$a = -\frac{M_C^{\text{ext}}}{a_{33} l}. \tag{40}$$

From (19) and (33), for reasons of symmetry, we simply have

$$\tau_1 = \tau_1^{\text{ext},A} = \tau_1^{\text{ext},C} = 0, \quad \tau_2 = \tau_2^{\text{ext},A} = \tau_2^{\text{ext},C} = -\frac{a_{33}}{2} a = \frac{1}{2l} M_C^{\text{ext}}. \tag{41}$$

From (19) and (33) we have

$\tau_1 = \tau_1^{\text{ext},B} = 0, \quad \tau_1 = \tau_1^{\text{ext},D} = 0,$

and we also have

$$\tau_2 = \tau_2^{B,\text{ext}} = -\frac{a_{13}}{\sqrt{2}} a, \quad \tau_2 = \tau_2^{D,\text{ext}} = \tau_2^{B,\text{ext}} = \frac{a_{13}}{a_{33}} \frac{M_C^{\text{ext}}}{l\sqrt{2}}. \tag{42}$$

We impose no kinematic restrictions on wedges. This means, again, that the external (or reaction) wedge force, in order to have the displacement field (33), is

$f_\alpha^{\text{ext}} = -T_{\alpha 12} - T_{\alpha 21}$

for wedges $\mathcal{V}_1$ and $\mathcal{V}_3$ and the converse

$f_\alpha^{\text{ext}} = T_{\alpha 12} + T_{\alpha 21}$

for wedges $\mathcal{V}_2$ and $\mathcal{V}_4$. We have from (22) and (33)

$$T_{112} + T_{121} = \frac{a}{2}\left(a_{33} + \sqrt{2} a_{23}\right) = -\frac{M_C^{\text{ext}}}{2l}\left(1 + \sqrt{2}\frac{a_{23}}{a_{33}}\right). \tag{43}$$

From (23) and (33), on the other hand, we simply have

$$T_{212} + T_{221} = 0. \tag{44}$$

3.5 An analytical solution for the trapezoidal case

Let us take into account the following displacement field (see also Fig. 5):

$$u_1 = 0, \quad u_2 = b X_1 X_2. \tag{45}$$

The two PDEs (15) and (16) are satisfied by the nonnull horizontal external force per unit area:

$b_1^{\text{ext}} = b\left(c_{12} + \frac{1}{2} c_{33}\right), \quad b_2^{\text{ext}} = 0.$

In what follows we consider the solution (45) and calculate the whole set of boundary conditions.

Journal: 10665-ENGI Article No.: 9856 MS Code: ENGI-D-15-00194.3 TYPESET DISK LE CP Disp.:2016/4/9 Pages: 21 Layout: Medium

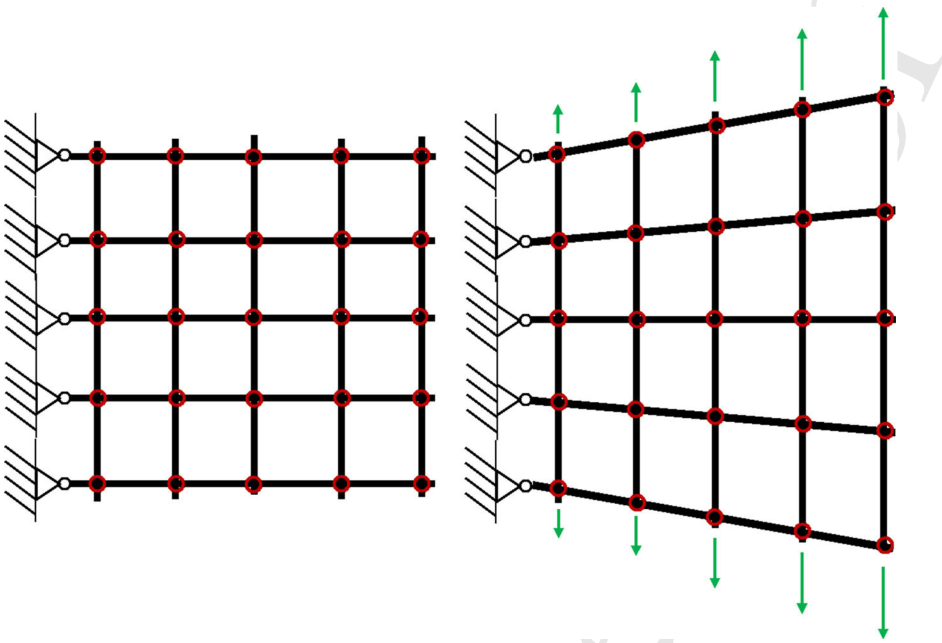

Fig. 5 Discrete pantographic structure in trapezoidal case. *Left-hand side*: reference configuration; *right-hand side*: deformation in trapezoidal condition

In particular, we calculate the edge forces and double forces that are necessary to have the displacement fields (45) and use the same convention to characterize each edge.

From (18) and (45) we have

$$t_1 = t_1^{\mathrm{ext},A} = 0, \quad t_2 = t_2^{\mathrm{ext},A} = -\frac{b}{2} c_{33} X_2, \tag{46}$$

and

$$t_1 = t_1^{\mathrm{ext},C} = b c_{12} L, \quad t_2 = t_2^{\mathrm{ext},C} = -t_2^{\mathrm{ext},A} = \frac{b}{2} c_{33} X_2. \tag{47}$$

From (18) we have

$$t_1^{\mathrm{ext},B} = t_1^{\mathrm{ext},D} = b\frac{c_{33} l}{2}, \quad t_2^{\mathrm{ext},B} = -t_2^{\mathrm{ext},D} = b c_{11} X_1. \tag{48}$$

From (19) and (45) we simply have

$\tau_2 = \tau_2^{\mathrm{ext},A} = \tau_2^{\mathrm{ext},C} = 0,$

i.e., null double force per unit length in the vertical direction for vertical sides, and we also have

$$\tau_1 = \tau_1^{\mathrm{ext},A} = \tau_1^{\mathrm{ext},C} = b\left(a_{12} + \frac{a_{13}}{\sqrt{2}}\right). \tag{49}$$

From (19) and (45) we have

$$\tau_1 = \tau_1^{\mathrm{ext},B} = \tau_1^{\mathrm{ext},D} = \frac{b}{2}(\sqrt{2} a_{23} + a_{33}), \;\; \tau_2 = \tau_2^{B,\mathrm{ext}} = \tau_2^{D,\mathrm{ext}} = 0. \tag{50}$$

Journal: 10665-ENGI Article No.: 9856 MS Code: ENGI-D-15-00194.3 TYPESET DISK LE CP Disp.:2016/4/9 Pages: 21 Layout: Medium

We impose no kinematic restrictions on wedges. This means, again, that the external (or reaction) wedge force, in order to have the displacement fields (45), is

$$f_\alpha^{\text{ext}} = -T_{\alpha 12} - T_{\alpha 21}$$

for wedges $\mathcal{V}_1$ and $\mathcal{V}_3$ and the converse

$$f_\alpha^{\text{ext}} = T_{\alpha 12} + T_{\alpha 21}$$

for wedges $\mathcal{V}_2$ and $\mathcal{V}_4$. We have from (22) and (45)

$$T_{112} + T_{121} = 0;$$

on the other hand we simply have

$$T_{212} + T_{221} = \frac{b}{2}\left(2a_{22} + 2\sqrt{2}a_{23} + a_{33}\right). \tag{51}$$

4 The pantographic case

Let us assume that the two families of fibers in the pantographic structure are aligned with the axes of the frame of reference. It would be convenient for the reader to have in mind the right-hand sides of Figs. 3, 4, and 5. A series of intuitive considerations is made in this section. In other words, a set of gedanken experiments is conceived for the purpose of parameter identification. First of all, in the heavy sheet case, we can prove not only that the vertical displacement of side D is

$$u_2(X_1, X_2 = -l) = \frac{2\rho g l^2}{c_{11}} = \frac{2\rho_m g l^2}{E_m}, \tag{52}$$

where ρ_m is the mass per unit volume of the microbeams and E_m is their Young's modulus, but also the relation

$$\rho = \frac{\rho_m A_m}{d_m}, \tag{53}$$

where A_m is the cross-sectional area of each microbeam and d_m is the distance between two adjacent families of microbeams. From (52) and (53) we have

$$c_{11} = E_m \frac{2\rho g l^2}{2\rho_m g l^2} = E_m \frac{\rho_m A_m}{d_m}\frac{1}{\rho_m} = \frac{E_m A_m}{d_m}. \tag{54}$$

Second, in the nonconventional bending case we set an equivalence of such a case with a series of a number $\left(\text{i.e., } \frac{2l}{d_m}\right)$ of conventional bending microbeams, so that the total external moment M_C^{ext} on side C is related to the external moment M_m on each microbeam,

$$M_C^{\text{ext}} = -\frac{2l}{d_m} M_m, \tag{55}$$

and the vertical displacement of side C is

$$u_2(X_1 = L, X_2) = -\frac{aL^2}{2} = -\frac{M_m L^2}{2E_m I_m}, \tag{56}$$

where I_m is the moment of inertia of the microbeams. Equations (40), (55), and (56) give

$$a_{33} = -\frac{M_C^{\text{ext}}}{al} = \frac{2l}{d_m} M_m \frac{1}{al} = \frac{2l}{d_m} \frac{aL^2 2E_m I_m}{2L^2} \frac{1}{al} = 2\frac{E_m I_m}{d_m}. \tag{57}$$

Further trivial considerations made from the particular pantographic structure in the heavy sheet configuration are made. First of all, the natural absence of the Poisson effect in this configuration makes the horizontal edge force per unit length on the vertical sides that are given from (28). This and (54) give

$$t_1^{\text{ext},C} = \frac{\rho g (l + X_2)}{c_{11}} c_{12} = 0 \;\Rightarrow\; c_{12} = 0. \tag{58}$$

Second, in the same heavy sheet configuration, the natural absence of a double force on the vertical sides gives, from (30) and (54),

$$\tau_2^{\text{ext},C} = \frac{a_{13}\rho g}{\sqrt{2}c_{11}} = 0 \;\Rightarrow\; a_{13} = 0. \tag{59}$$

Note that the identification that is made explicit in (59) can also be achieved assuming zero double force on the horizontal sides for the nonconventional bending case from (42).

In addition, in the same heavy sheet configuration, the natural absence of double force on the horizontal sides gives from (31) and (54)

$$\tau_2^{D,\text{ext}} = \frac{\rho g a_{11}}{c_{11}} = 0 \;\Rightarrow\; a_{11} = 0. \tag{60}$$

Moreover, in the same heavy sheet configuration, the natural absence of wedge forces gives, from (32) and (54),

$$T_{112} + T_{121} = \frac{\left(2a_{12} + \sqrt{2}a_{13}\right)\rho g}{2c_{11}} = 0 \;\Rightarrow\; 2a_{12} + \sqrt{2}a_{13} = 0. \tag{61}$$

Note that the identification that is made explicit in (61) can also be achieved assuming zero horizontal double force in the trapezoidal case on the vertical sides from (49).

It is also convenient to consider, in the nonconventional bending case, the fact that the external force per unit area must be zero. Thus, from (34) we have

$$b_2^{\text{ext}} = -\frac{a}{2} c_{33} = 0 \;\Rightarrow\; c_{33} = 0. \tag{62}$$

Note that the identification that is made explicit in (62) can also be achieved assuming, in the nonconventional bending case, zero horizontal force per unit length on the vertical sides from $(35)_1$ or from $(36)_1$ or assuming zero horizontal force per unit length on the horizontal sides from (37) or, in the trapezoidal case, by assuming zero vertical force per unit length on the vertical sides from $(46)_2$ and $(47)_2$ or zero horizontal force per unit length on the horizontal sides from (48).

Moreover, in the nonconventional bending case, the natural absence of wedge forces gives, from (43),

$$T_{112} + T_{121} = \frac{a}{2}\left(a_{33} + \sqrt{2}a_{23}\right) = 0 \;\Rightarrow\; a_{33} + \sqrt{2}a_{23} = 0. \tag{63}$$

Note that the identification that is made explicit in (63) can also be achieved assuming zero horizontal double force in the trapezoidal case on the horizontal sides from (50).

Journal: 10665-ENGI Article No.: 9856 MS Code: ENGI-D-15-00194.3 TYPESET DISK LE CP Disp.:2016/4/9 Pages: 21 Layout: Medium

Finally, assuming zero wedge forces in the trapezoidal case, we have from (51)

$$T_{212} + T_{221} = \frac{b}{2}\left(2a_{22} + 2\sqrt{2}a_{23} + a_{33}\right) = 0 \;\Rightarrow\; 2a_{22} + 2\sqrt{2}a_{23} + a_{33} = 0. \tag{64}$$

Equations (54), (57), (58), (59), (60), (61), (62), (63), and (64) completely characterize the orthotropic material. In particular, the two constitutive matrices are represented as follows:

$$\mathbf{C} = \frac{E_m A_m}{d_m}\begin{pmatrix} 1 & 0 & 0 \\ 0 & 1 & 0 \\ 0 & 0 & 0 \end{pmatrix}, \quad \mathbf{A} = \frac{E_m I_m}{d_m}\begin{pmatrix} 0 & 0 & 0 & 0 & 0 & 0 \\ 0 & 1 & -\sqrt{2} & 0 & 0 & 0 \\ 0 & -\sqrt{2} & 2 & 0 & 0 & 0 \\ 0 & 0 & 0 & 0 & 0 & 0 \\ 0 & 0 & 0 & 0 & 1 & -\sqrt{2} \\ 0 & 0 & 0 & 0 & -\sqrt{2} & 2 \end{pmatrix}. \tag{65}$$

It is interesting to recognize that the internal energy (8) can now be computed using (9), (10) and using the definition, in the linear case, of the deformation matrix G and of its gradient ∇G:

$$\begin{aligned} U(G, \nabla G) = {} & \frac{1}{2}\frac{E_m A_m}{d_m}\left(G_{11}^2 + G_{22}^2\right) + \frac{1}{2}\frac{E_m I_m}{d_m}\left[G_{22,1}\left(G_{22,1} - 2G_{12,2}\right) + 2G_{12,2}\left(-G_{22,1} + 2G_{12,2}\right)\right] \\ & + \frac{1}{2}\frac{E_m I_m}{d_m}\left[G_{11,2}\left(G_{11,2} - 2G_{12,1}\right) + 2G_{12,1}\left(-G_{11,2} + 2G_{12,1}\right)\right], \end{aligned}$$

or, in terms of the displacement field,

$$U(G, \nabla G) = \frac{E_m A_m}{2d_m}\left(u_{1,1}^2 + u_{2,2}^2\right) + \frac{1}{2}\frac{E_m I_m}{d_m}\left(u_{1,22}^2 + u_{2,11}^2\right). \tag{66}$$

Expression (66) is a remarkable form of the energy. It simply resembles the contributions of both series of fibers for axial and for bending deformations of the microbeams. Note, finally, that expression (66) is not compatible with that derived in [99], where the authors aimed only at proving the necessity of a second gradient energy for pantographic continua and not for the related parameter identification in terms of microstructural characteristics. On the basis of this simple strain energy function, we show in the next section numerical simulations that confirm the validity of the model.

5 Numerical simulations

In the numerical simulations in this section we will not simply refer to the rectangle in Fig. 2; we will refer to it—but rotated by 45°. The fibers are aligned, in the nondeformed configuration, along the horizontal and vertical directions, not along the rectangle's sides.

In Fig. 6 a displacement of the short side of the rectangle in the direction of its long side is shown, and the result is a classic bone-shaped deformation. In Fig. 7 a displacement is prescribed, in the direction of the short side of the rectangle, to the single vertex on the left-hand side, a zero displacement is applied at the bottom vertex, and a floppy mode is shown.

4

In Fig. 6a is shown the deformation of the fibers, even though the model is a continuum, in the numerical bias test, where the color indicates the deformation energy density. Note the concentration of the deformation energy density around the corners and the classic bone shape of the deformation of the body. The same bone shape is also shown in Fig. 6b, where colors indicate the shear deformation G_{12} and where we refer to the same boundary value problem. In Fig. 7 the floppy mode is shown. In this case the color indicates the deformation energy density and the scale makes clear that for a high deformation level we have practically zero deformation energy.

Journal: 10665-ENGI Article No.: 9856 MS Code: ENGI-D-15-00194.3 TYPESET DISK LE CP Disp.:2016/4/9 Pages: 21 Layout: Medium

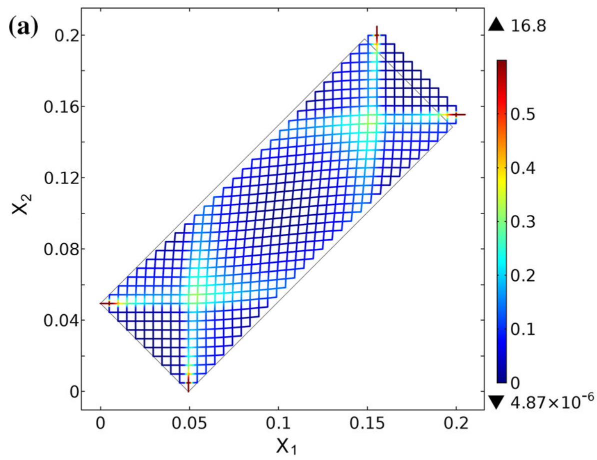

Fig. 6 Bias test. In both panels a representation of the numerical results on the continuum model is presented. **a** Deformation of fibers (*color*: deformation energy density) in the continuum model of the pantographic structure. The directions of the fibers represent the privileged directions of the orthotropic continuum model; they are not a graphical representation of any simulated discrete model. **b** Deformation of continuum pantographic structure (*colors*: shear deformation G_{12})

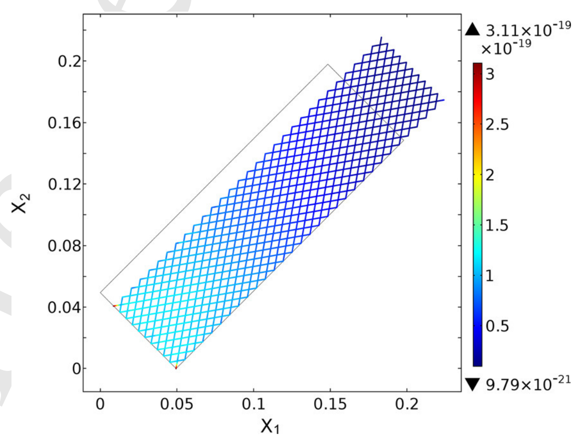

Fig. 7 Floppy mode: deformation of fibers (*color*: deformation energy density) in continuum model of pantographic structure

To show the presence of a boundary layer, we illustrate in Fig. 8b the second derivative $u_{1,22}$ of the first displacement component u_1 with respect to the second coordinate X_2, as a function of a third coordinate s characterizing each point of the cut represented in Fig. 8a. Note that on the one hand, because of the high axial rigidity of each microbeam of the pantographic structure, for small values of the coordinate s the deformation regime is almost rigid and the strain gradient component $u_{1,22}$ is almost zero. For high values of the same coordinate s, on the other hand, the component $u_{1,22}$ is much higher. Thus, a transition zone can be ~~appreciated~~. Such a transition zone is the 5
so-called boundary layer of the problem. The thickness of such a boundary layer is proportional to the ratio between the second and first gradient parameters. In Fig. 8b different boundary layers are numerically evaluated for different values of the second gradient parameters. In particular, we show the results for the identified value of the second gradient parameter in terms of the moment of inertia of the sections of the microbeams, as well the results for lower (one tenth and one hundredth times) and for higher (ten and one hundred times) values of such a moment of inertia. Finally, it is worth noting that it is confirmed that the largeness of the boundary layers is effectively proportional to the second gradient parameters, in the sense that the higher the second gradient parameters, the larger the boundary 6
layer. 7

Journal: **10665-ENGI** Article No.: **9856** MS Code: **ENGI-D-15-00194.3** TYPESET DISK LE CP Disp.:**2016/4/9** Pages: **21** Layout: **Medium**

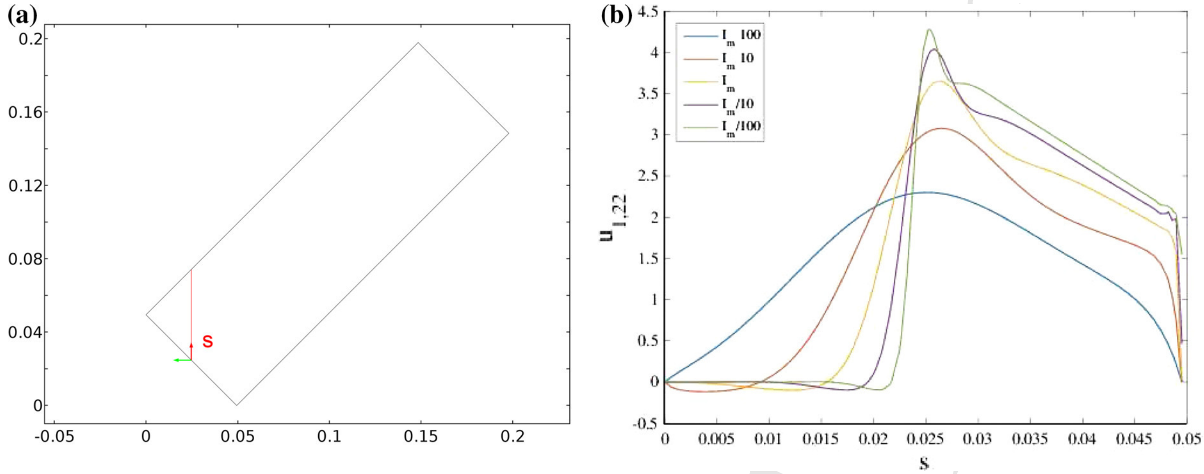

Fig. 8 Boundary layer. **a** On the *left-hand side* we show the cut on which we calculate $u_{1,22}$, represented on the *right-hand side* (**b**). In addition, on the *right-hand side*, we show the numerical simulations calculated using different moments of inertia I_m given in the legend of Fig. 8b

6 Conclusion

In this paper we have identified the whole set of nine parameters of a homogeneous linear elastic second gradient orthotropic D_4 material, which is the most general symmetry that is valid for pantographic structures with two identical and orthogonal families of fibers. Analytical solutions were developed and shown and, as a consequence, the identification was done in terms of the Young's modulus of the fiber material, of the area, and of the moment of inertia of the cross sections of the fibers and the distance between the nearest pivots. A remarkable form of the strain energy that closely resembles the strain energy of simple Euler beams was derived in terms of the displacement field. Numerical simulations confirmed the validity of the presented model. In fact, a bone-shaped deformation, in a proper bias test, was obtained, as was a continuum floppy mode, which is a deformation mode with finite deformation and zero deformation energy. Finally, we also showed the dependence of the largeness of the boundary layer with respect to the second gradient coefficients of the model.

Acknowledgments We thank Prof. Francesco dell'Isola and Prof. Pierre Seppecher for fruitful discussions on the theoretical foundations of the continuum model used in this paper, on the importance of pantographic structures in the field of microstructured continua, and on some special technical topics in this manuscript. We also would like to thank the anonymous reviewer who helped to improve the quality of this manuscript.

References

1. dell'Isola F, Lekszycki T, Pawlikowski M, Grygoruk R, Greco L (2015) Designing a light fabric metamaterial being highly macroscopically tough under directional extension: first experimental evidence. Z Angew Math Phys 66(6):3473–3498
2. Seppecher P, Alibert J-J, dell'Isola F (2011) Linear elastic trusses leading to continua with exotic mechanical interactions. J Phys Conf Ser 319(1):1–13
3. Naumenko K, Eremeyev VA (2014) A layer-wise theory for laminated glass and photovoltaic panels. Compos Struct 112(1):283–291
4. Rosi G, Giorgio I, Eremeyev VA (2013) Propagation of linear compression waves through plane interfacial layers and mass adsorption in second gradient fluids. Z Angew Math Mech (ZAMM) 93(12):914–927
5. Steigmann DJ, Pipkin AC (1989) Wrinkling of pressurized membranes. J Appl Mech Trans ASME 56(3):624–628
6. Steigmann DJ, Pipkin AC (1989) Finite deformations of wrinkled membranes. Q J Mech Appl Math 42(3):427–440
7. Steigmann DJ, Pipkin AC (1989) Axisymmetric tension fields. Z Angew Math Phys (ZAMP) 40(4):526–542
8. Bo P, Wang W (2007) Geodesic-controlled developable surfaces for modeling paper bending. Comput Graph Forum 26(3):365–374
9. Garay ÓJ, Tazawa Y (2015) Extremal curves for weighted elastic energy in surfaces of 3-space forms. Appl Math Comput 251:349–362

10. Steigmann DJ, dell'Isola F (2015) Mechanical response of fabric sheets to three-dimensional bending, twisting, and stretching. Acta Mech Sin 31(3):373–382
11. Luongo A, D'Annibale F (2012) Bifurcation analysis of damped visco-elastic planar beams under simultaneous gravitational and follower forces. Int J Mod Phys B 26(25):art. no. 1246015
12. Rizzi NL, Varano V (2011) The effects of warping on the postbuckling behaviour of thin-walled structures. Thin-Walled Struct 49(9):1091–1097
13. Ruta GC, Varano V, Pignataro M, Rizzi NL (2008) A beam model for the flexural-torsional buckling of thin-walled members with some applications. Thin-Walled Struct 46(7):816–822
14. Goda I, Rahouadj R, Ganghoffer J-F (2013) Size dependent static and dynamic behavior of trabecular bone based on micromechanical models of the trabecular architecture. Int J Eng Sci 72:53–77
15. Rinaldi A, Mastilovic S (2014) The Krajcinovic approach to model size dependent fracture in quasi-brittle solids. Mech Mater 71:21–33
16. Sansour C, Skatulla S (2009) A strain gradient generalized continuum approach for modelling elastic scale effects. Comput Methods Appl Mech Eng 198(15):1401–1412
17. Neff P, Jeong J, Ramézani H (2009) Subgrid interaction and micro-randomness—novel invariance requirements in infinitesimal gradient elasticity. Int J Solids Struct 46(25):4261–4276
18. Baraldi D, Reccia E, Cazzani A, Cecchi A (2013) Comparative analysis of numerical discrete and finite element models: the case of in-plane loaded periodic brickwork. Composites 4(4):319–344
19. Bilotta A, Turco E (2009) A numerical study on the solution of the Cauchy problem in elasticity. Int J Solids Struct 46(25–26):4451–4477
20. Cazzani A, Ruge P (2012) Numerical aspects of coupling strongly frequency-dependent soil-foundation models with structural finite elements in the time-domain. Soil Dyn Earthq Eng 37:56–72
21. Cesarano C, Assante D (2014) A note on generalized Bessel functions. Int J Math Models Methods Appl Sci 8(1):38–42
22. Della Corte A, Battista A, dell'Isola F (2015) Referential description of the evolution of a 2D swarm of robots interacting with the closer neighbors: perspectives of continuum modeling via higher gradient continua. Int J Non-Linear Mech. doi:10.1016/j.ijnonlinmec.2015.06.016
23. Garusi E, Tralli A, Cazzani A (2004) An unsymmetric stress formulation for Reissner–Mindlin plates: a simple and locking-free rectangular element. Int J Comput Eng Sci 5(3):589–618
24. Greco L, Cuomo M (2014) Consistent tangent operator for an exact Kirchhoff rod model. Contin Mech Thermodyn 25:861–877
25. Greco L, Cuomo M (2014) An implicit G1 multi patch B-spline interpolation for Kirchhoff–Love space rod. Comput Methods Appl Mech Eng 269:173–197
26. Selvadurai APS, Nguyen TS (1993) Finite element modelling of consolidation of fractured porous media. In: Canadian geotechnical conference, pp 361–370
27. Terravecchia S, Panzeca T, Polizzotto C (2014) Strain gradient elasticity within the symmetric BEM formulation. Fract Struct Integr 29:61–73
28. dell'Isola F, Andreaus U, Placidi L (2015) At the origins and in the vanguard of peri-dynamics, non-local and higher gradient continuum mechanics. An underestimated and still topical contribution of Gabrio Piola, Mechanics and Mathematics of Solids (MMS) 20:887–928
29. Alibert J-J, Corte AD (2015) Second-gradient continua as homogenized limit of pantographic microstructured plates: a rigorous proof. Z Angew Math Phys 66(5):2855–2870
30. Cecchi A, Rizzi NL (2001) Heterogeneous elastic solids: a mixed homogenization-rigidification technique. Int J Solids Struct 38(1):29–36
31. dell'Isola F, Seppecher P (2011) Commentary about the paper Hypertractions and hyperstresses convey the same mechanical information. Continuum Mec. Thermodyn. 22:163-176 by Prof. Podio Guidugli and Prof. Vianello and some related papers on higher gradient theories. Contin Mech Thermodyn 23(5):473–478
32. Misra A, Singh V (2015) Thermomechanics-based nonlinear rate-dependent coupled damage-plasticity granular micromechanics model. Contin Mech Thermodyn 27(4):787–817
33. Altenbach H, Eremeev VA, Morozov NF (2010) On equations of the linear theory of shells with surface stresses taken into account. Mech Solids 45(3):331–342
34. Cuomo M, Contrafatto L, Greco L (2014) A variational model based on isogeometric interpolation for the analysis of cracked bodies. Int J Eng Sci 80:173–188
35. D'Annibale F, Luongo A (2013) A damage constitutive model for sliding friction coupled to wear. Contin Mech Thermodyn 25(2–4):503–522
36. Placidi L (2016) A variational approach for a nonlinear one-dimensional damage-elasto-plastic second-gradient continuum model. Contin Mech Thermodyn 28:119–137
37. Placidi L (2015) A variational approach for a nonlinear 1-dimensional second gradient continuum damage model. Contin Mech Thermodyn 27:623–638
38. Roveri N, Carcaterra A, Akay A (2009) Vibration absorption using non-dissipative complex attachments with impacts and parametric stiffness. J Acoust Soc Am 126(5):2306–2314
39. Yang Y, Ching WY, Misra A (2011) Higher-order continuum theory applied to fracture simulation of nanoscale intergranular glassy film. J Nanomech Micromech 1(2):60–71

Journal: 10665-ENGI Article No.: 9856 MS Code: ENGI-D-15-00194.3 ☐ TYPESET ☐ DISK ☐ LE ☐ CP Disp.:2016/4/9 Pages: 21 Layout: Medium

40. Dos Reis F, Ganghoffer JF (2012) Construction of micropolar continua from the asymptotic homogenization of beam lattices. Comput Struct 112–113:354–363
41. Goda I, Assidi M, Ganghoffer JF (2014) A 3D elastic micropolar model of vertebral trabecular bone from lattice homogenization of the bone microstructure. Biomech Model Mechanobiol 13(1):53–83
42. Madeo A, Neff P, Ghiba I-D, Placidi L, Rosi G (2015) Band gaps in the relaxed linear micromorphic continuum. J Appl Math Mech (Z Angew Math Mech) 95:880–887
43. Piccardo G, Ranzi G, Luongo A (2014) A complete dynamic approach to the generalized beam theory cross-section analysis including extension and shear modes. Math Mech Solids 19(8):900–924
44. Mindlin RD (1964) Micro-structure in linear elasticity. Department of Civil Engineering, Columbia University, New York
45. dell'Isola F, Madeo A, Placidi L (2012) Linear plane wave propagation and normal transmission and reflection at discontinuity surfaces in second gradient 3D continua. J Appl Math Mech (Z Angew Math Mech) 92(1):52–71
46. dell'Isola F, Seppecher P, Della Corte A (2015) The postulations à la D' Alembert and à la Cauchy for higher gradient continuum theories are equivalent: a review of existing results. Proc R Soc Lond A 471(2183):20150415
47. Ferretti M, Madeo A, dell'Isola F, Boisse P (2014) Modelling the onset of shear boundary layers in fibrous composite reinforcements by second gradient theory. Z Angew Math Phys (ZAMP) 65(3):587–612
48. Madeo A, dell'Isola F, Darve F (2013) A continuum model for deformable, second gradient porous media partially saturated with compressible fluids. J Mech Phys Solids 61(11):2196–2211
49. dell'Isola F, Gouin H, Seppecher P (1995) Radius and surface tension of microscopic bubbles by second gradient theory. Comptes Rendus Acad Sci Ser IIb Mecc Phys Chim Astron 320(6):211–216
50. dell'Isola F, Gouin H, Rotoli G (1996) Nucleation of spherical shell-like interfaces by second gradient theory: numerical simulations. Eur J Mech B 15(4):545–568
51. dell'Isola F, Rotoli G (1995) Validity of Laplace formula and dependence of surface tension on curvature in second gradient fluids. Mech Res Commun 22(5):485–490
52. dell'Isola F, Sciarra G, Vidoli S (2009) Generalized Hooke's law for isotropic second gradient materials. R Soc Lond 465(107):2177–2196
53. dell'Isola F, Seppecher P (1997) Edge contact forces and quasi-balanced power. Meccanica 32(1):33–52
54. dell'Isola F, Seppecher P (1995) The relationship between edge contact forces, double forces and interstitial working allowed by the principle of virtual power. Comptes Rendus Acad Sci Ser IIb Mecc Phys Chim Astron 321:303–308
55. dell'Isola F, Guarascio M, Hutter K (2000) A variational approach for the deformation of a saturated porous solid. A second-gradient theory extending Terzaghi's effective stress principle. Arch Appl Mech 70(5):323–337
56. dell'Isola F, Madeo A, Seppecher P (2009) Boundary conditions at fluid-permeable interfaces in porous media: a variational approach. Int J Solids Struct 46(17):3150–3164
57. dell'Isola F, Sciarra G, Batra R (2005) A second gradient model for deformable porous matrices filled with an inviscid fluid. Solid mechanics and its applications—IUTAM symposium on physicochemical and electromechanical interactions in porous media, vol 125, pp 221–229
58. dell'Isola F, Sciarra G, Batra R (2003) Static deformations of a linear elastic porous body filled with an inviscid fluid. J Elasticity 72(1–2):99–120
59. Madeo A, dell'Isola F, Ianiro N, Sciarra G (2008) A variational deduction of second gradient poroelasticity II: an application to the consolidation problem. J Mech Mater Struct 3(4):607–625
60. Sciarra G, dell'Isola F, Coussy O (2007) Second gradient poromechanics. Int J Solids Struct 44(20):6607–6629
61. Sciarra G, dell'Isola F, Ianiro N, Madeo A (2008) A variational deduction of second gradient poroelasticity, part I: general theory. J Mech Mater Struct 3(3):507–526
62. Yang Y, Misra A (2012) Micromechanics based second gradient continuum theory for shear band modeling in cohesive granular materials following damage elasticity. Int J Solids Struct 49(18):2500–2514
63. Alibert J, Seppecher P, dell'Isola F (2003) Truss modular beams with deformation energy depending on higher displacement gradients. Math Mech Solids 8(1):51–73
64. dell'Isola F, Steigmann D (2015) A two-dimensional gradient-elasticity theory for woven fabrics. J Elasticity 118(1):113–125
65. Rinaldi A, Placidi L (2015) A microscale second gradient approximation of the damage parameter of quasi-brittle heterogeneous lattices. J Appl Math Mech (Z Angew Math Mech) 94:862–877
66. de Oliveira Góes RC, de Castro JTP, Martha LF (2014) 3D effects around notch and crack tips. Int J Fatigue 62:159–170
67. Del Vescovo D, Giorgio I (2014) Dynamic problems for metamaterials: review of existing models and ideas for further research. Int J Eng Sci 80:153–172
68. dell'Isola F, Della Corte A, Greco L, Luongo A (2016) Plane bias extension test for a continuum with two inextensible families of fibers: a variational treatment with Lagrange Multipliers and a perturbation solution. Int J Solids Struct 81:1–12
69. Madeo A, Della Corte A, Greco L, Neff P (2015) Wave propagation in pantographic 2D lattices with internal discontinuities. Proc Estonian Acad Sci 64(3S):325–330
70. dell'Isola F, Della Corte A, Giorgio I, Scerrato D (2015) Pantographic 2D sheets: discussion of some numerical investigations and potential applications. Int J Non-Linear Mech 80:200–208
71. Piccardo G, Pagnini LC, Tubino F (2014) Some research perspectives in galloping phenomena: critical conditions and post-critical behavior. Contin Mech Thermodyn 27(1–2):261–285
72. Auffray N (2015) On the isotropic moduli of 2D strain-gradient elasticity. Contin Mech Thermodyn 27(1–2):5–19

Journal: 10665-ENGI Article No.: 9856 MS Code: ENGI-D-15-00194.3 TYPESET DISK LE CP Disp.:2016/4/9 Pages: 21 Layout: Medium

73. Placidi L, Andreaus U, Della Corte A, Lekszycki T (2015) Gedanken experiments for the determination of two-dimensional linear second gradient elasticity coefficients. Z Angew Math Phys 66:3699–3725
74. Auffray N, Dirrenberger J, Rosi G (2015) A complete description of bi-dimensional anisotropic strain-gradient elasticity. Int J Solids Struct 69—-70:195–206
75. Goda I, Assidi M, Belouettar S, Ganghoffer JF (2012) A micropolar anisotropic constitutive model of cancellous bone from discrete homogenization. J Mech Behav Biomed Mater 16(1):87–108
76. Misra A, Huang S (2012) Micromechanical stress-displacement model for rough interfaces: effect of asperity contact orientation on closure and shear behavior. Int J Solids Struct 49(1):111–120
77. Selvadurai PA, Selvadurai APS (2014) On the effective permeability of a heterogeneous porous medium: the role of the geometric mean. Philos Mag 94(20):2318–2338
78. Misra A, Poorsolhjouy P (2013) Micro-macro scale instability in 2D regular granular assemblies. Contin Mech Thermodyn 27(1–2):63–82
79. Presta F, Hendy CR, Turco E (2008) Numerical validation of simplified theories for design rules of transversely stiffened plate girders. Struct Eng 86(21):37–46
80. Rinaldi A (2009) Rational damage model of 2D disordered brittle lattices under uniaxial loadings. Int J Damage Mech 18(3):233–257
81. Solari G, Pagnini LC, Piccardo G (1997) A numerical algorithm for the aerodynamic identification of structures. J Wind Eng Ind Aerodyn 69–71:719–730
82. Turco E (2013) Identification of axial forces on statically indeterminate pin-jointed trusses by a nondestructive mechanical test. Open Civ Eng J 7(1):50–57
83. Eremeyev VA, Pietraszkiewicz W (2006) Local symmetry group in the general theory of elastic shells. J Elasticity 85(2):125–152
84. Eremeyev VA, Pietraszkiewicz W (2012) Material symmetry group of the non-linear polar-elastic continuum. Int J Solids Struct 49(14):1993–2005
85. Placidi L, El Dhaba AR. Semi-inverse method à la Saint-Venant for two-dimensional linear isotropic homogeneous second gradient elasticity. Mech Math Solids (in press) 8
86. Armstrong MA (1983) Basic topology. Springer, New York
87. Auffray N, Bouchet R, Brechet Y (2009) Derivation of anisotropic matrix for bi-dimensional strain-gradient elasticity behavior. Int J Solids Struct 46(2):440–454
88. Auffray N, Kolev B, Petitot M (2014) On anisotropic polynomial relations for the elasticity tensor. J Elasticity 115(1):77–103
89. Indelicato G, Albano A (2009) Symmetry properties of the elastic energy of a woven fabric with bending and twisting resistance. J Elasticity 94(1):33–54
90. Federico S (2010) On the linear elasticity of porous materials. Int J Mech Sci 52(2):175–182
91. Federico S (2012) Covariant formulation of the tensor algebra of non-linear elasticity. Int J Non-Linear Mech 47(2):273–284
92. Federico S (2010) Volumetric-distortional decomposition of deformation and elasticity tensor. Math Mech Solids 15(6):672–690
93. Federico S, Grillo A, Herzog W (2004) A transversely isotropic composite with a statistical distribution of spheroidal inclusions: a geometrical approach to overall properties. J Mech Phys Solids 52(10):2309–2327
94. Federico S, Grillo A, Imatani S (2015) The linear elasticity tensor of incompressible materials. Math Mech Solids 20(6):643–662
95. Federico S, Grillo A, Wittum G (2009) Considerations on incompressibility in linear elasticity. Nuovo Cimento C 32C(1):81–87
96. Hill R (1965) A self-consistent mechanics of composite materials. J Mech Phys Solids 13:213–222
97. Walpole LJ (1981) Elastic behavior of composite materials: theoretical foundations. Adv Mech 21:169–242
98. Walpole LJ (1984) Fourth-rank tensors of the thirty-two crystal classes: multiplication tables. Proc R Soc Lond Ser A 391:149–179
99. Rahali Y, Giorgio I, Ganghoffer JF, dell'Isola F (2015) Homogenization à la Piola produces second gradient continuum models for linear pantographic lattices. Int J Eng Sci 97:148–172

Journal: **10665-ENGI** Article No.: **9856** MS Code: **ENGI-D-15-00194.3** ☐ TYPESET ☐ DISK ☐ LE ☐ CP Disp.:**2016/4/9** Pages: **21** Layout: **Medium**

Journal: 10665
Article: 9856

Author Query Form

Please ensure you fill out your response to the queries raised below and return this form along with your corrections

Dear Author

During the process of typesetting your article, the following queries have arisen. Please check your typeset proof carefully against the queries listed below and mark the necessary changes either directly on the proof/online grid or in the 'Author's response' area provided below

Query	Details required	Author's response
1.	AQ: Please confirm changes in this sentence. (It was changed so that both "the presence of..." and "interactions between" consitute necessary ingredients..." In the original, it wasn't clear whether "the presence of..." also related to "necessary ingredients...," though it seemed like that was the intention.)	We confirm, thanks.
2.	AQ: Inserted "partial differential equation" as the definition of "PDE." Please confirm.	We confirm, thanks.
3.	AQ: Changed "given" to "derived." Please confirm.	We confirm, thanks.
4.	As per the information provided by the publisher, Figs. 6 and 7 will be black and white in print; hence, please confirm whether we can add 'colour figure online' to the caption.	Yes, please, add "colour figure online" to the caption
5.	AQ: The use of "appreciated" is unclear. Do you mean "discerned" or "identified"? Please revise.	We mean "discerned"
6.	AQ: Replaced "higher the largeness of" with "larger." Please confirm.	We confirm
7.	Figure 8a is poor in quality as its labels are not readable. Please supply a new version of the said figure with legible labels preferably in .eps, .tiff or .jpeg format with 600 dpi resolution.	We attach the Fig. 8a in jpeg format with 600 dpi resolution
8.	Please update Ref. [85].	We add the doi. The paper still does not have an issue number. The doi is the following: 10.1177/1081286515616043